Front. Energy 2021, 15(3): 687–699
https://doi.org/10.1007/s11708-021-0773-9

RESEARCH ARTICLE

Qingyu WEI, Yao WANG, Bin DAI, Yan YANG, Haijun LIU, Huaijie YUAN, Dengwei JING, Liang ZHAO

Theoretical study on flow and radiation in tubular solar photocatalytic reactor

Abstract In this paper, based on the mixture flow model, an optimized six-flux model is first established and applied to the tubular solar photocatalytic reactor. Parameters influencing photocatalyst distribution and radiation distribution at the reactor outlet, viz. catalyst concentration and circulation speed, are also analyzed. It is found that, at the outlet of the reactor, the optimized six-flux model has better performances (the energy increase by 1900% and 284%, respectively) with a higher catalyst concentration (triple) and a lower speed (one third).

Keywords photocatalytic hydrogen photoreactor, numerical simulation, solar energy, flow model, radiation model

1 Introduction

Presently, fossil energy is the most important energy source, but its exploitation and utilization process have caused serious environmental pollution and brought about irreversible ecological damage. Therefore, it is necessary to develop renewable and clean energy sources [1–6]. Hydrogen energy is recognized as one of the most superior energy carriers in the world [1–9] because of its high energy density, convenient storage and transportation, and no pollution of combustion products. At the same time, solar energy is abundant and clean [10]. Nowadays, the efficient conversion of solar energy to hydrogen energy has become one of the effective ways to solve the energy and environment problems. For the direct solar photocatalytic hydrogen production reactor, the flow characteristics and radiation distribution in the reactor are the focus of study. It is a difficult to establish the numerical model coupling flow field with radiation field in the reactor. Therefore, relevant theoretical research in this field is rarely reported.

1.1 Flow numerical simulation research

In the process of photocatalysis, flow field is the precondition of radiation field. The study of the flow field in the photocatalytic reactor can be simplified to the liquid-solid two phase flow model in essence. With the development of the computer technology, computational fluid dynamics (CFD) has become an important means of engineering application and designing. At this stage, there are two major models to describe multiphase flow: the Euler-Euler (E-E) model and the Euler-Lagrange (E-L) model. In particular, three different models are provided for the E-E model: the VOF (Volume of fluid), the mixture (mixture model), and the Eulerian (Euler model). Much work has been done on the study of liquid-solid flow in photocatalytic reaction. Kumar and Bansal [11] applied CFD to the photocatalytic process for the first time in 2013. The photocatalytic degradation device was modeled and the polynomial of degradation rate related to the initial concentration, Reynolds number, and reaction time were obtained. Ren and Jing [12] analyzed the differences between the E-E model and the E-L model in computational fluid dynamics (CFD). At the same time, the small

Received Jan. 10, 2021; accepted Jun. 9, 2021; online Sept. 10, 2021

Qingyu WEI
International Research Center for Renewable Energy, State Key Laboratory of Multiphase Flow in Powering Engineering, Xi'an Jiaotong University, Xi'an 710049, China; Beijing Aerospace Propulsion Institute, Beijing 100076, China

Yao WANG, Bin DAI, Haijun LIU, Huaijie YUAN, Dengwei JING, Liang ZHAO (✉)
International Research Center for Renewable Energy, State Key Laboratory of Multiphase Flow in Powering Engineering, Xi'an Jiaotong University, Xi'an 710049, China
E-mail: lzhao@mail.xjtu.edu.cn

Yan YANG
International Research Center for Renewable Energy, State Key Laboratory of Multiphase Flow in Powering Engineering, Xi'an Jiaotong University, Xi'an 710049, China; School of Energy and Power Engineering, University of Shanghai for Science and Technology, Shanghai 200093, China

Special Issue—Photocatalysis: From Solar Light to Hydrogen Energy (Guest Editors: Wenfeng SHANGGUAN, Akihiko KUDO, Zhi JIANG, Yuichi YAMAGUCHI)

cylinder photocatalytic reactor was simulated by using the E-L model under the condition of agitation. The effects of stirring speed and particle size on the flow were analyzed. Ren et al. [13] also used the algebraic slip mixed model (ASM) to simulate the catalyst-fluid two phase flow in the reaction tube. The simulation results showed that the catalyst could remain suspended in the pipeline, within the range of the study, when the inlet velocity was above 0.06 m/s and the catalyst particle size was below 10 μm.

1.2 Radiation numerical simulation research

Radiation distribution in the photocatalytic reactor [14–18] is another important research. In essence, the calculation of the radiation distribution in the reactor is to obtain the local volume rate of photon absorption (LVRPA) of the reaction region by solving the radiative transfer equation (RTE). Many researchers have simplified the RTE equation, and the common simplified calculation methods are as follows:

1) The discrete coordinate method (DOM)

The DOM is reasonably discretized in the direction of radiation intensity. The exact solution is obtained by solving the RTE equation in the discrete direction [19];

2) The Monte Carlo method (MC)

The MC uses the probability and statistics method to simulate the interior of photocatalytic reactor;

3) The two-flux model (TFM)

The TFM assumes that the radiation field in the photocatalytic reactor is isotropic, and the catalyst has absorption and reflection effects on the radiation. The radiation intensity of a point in the reactor is the sum of the forward and backward radiation along the direction of incident light [20];

4) The six-flux model (SFM)

The SFM is aimed at the upgrade and improvement of TFM. It is considered that the radiation field in the photocatalytic reactor is anisotropic.

In addition to the consideration of TFM, the scattering in the left, right, up and down directions should also be considered [21]. A large number of computing efforts aimed at obtaining LVRPA have been conducted. Romero et al. [22] used DOM to simulate the cylindrical photocatalytic reactor with the light source in the center of the cylinder. The distribution of LVRPA in the reaction region of the reactor was obtained. Based on the calculation results, the theoretical basis for the design of cylindrical photocatalytic reactor was provided. Jing et al. [23] used MC to simulate the cylindrical fluidized bed photocatalytic reactor. The results showed that the uneven distribution of catalyst particles affected the light intensity of the reactor, and the optimum theoretical thickness in the reactor design was obtained. Brucato et al. [24] proposed a new six-flux model (SFM) which assumed that photons were scattered in six directions along the Cartesian coordinate system. At the same time, MC, TFM, and SFM were used to simulate the flat-plate photocatalytic reactor. It was found that the calculation results of these three models were consistent and the solution of SFM was more accurate.

In summary, complex optical, physics, and chemistry are involved in the solar photocatalytic hydrogen production reactor. Therefore, it is particularly critical to deeply explore the characteristics and laws of the flow and the radiation in the reactor of the solar photocatalytic water hydrogen production system. In this paper, the flow and radiation distribution in the circular tube photocatalytic reactor are investigated.

2 Model description

2.1 Flow model

As the photocatalytic reaction takes place, tiny hydrogen bubbles are formed at the liquid-solid mixing interface. But the volume fraction of these bubbles is very small, which will not have much impact on the mainstream. Therefore, the mixing bubble disturbance at the solid-liquid interface is ignored in this paper. The inner-flow reactor with liquid-solid two-phase flow is simplified. Flow and liquid-solid studies are relatively mature at present. In this paper, the mixture model is used to simulate the liquid-solid two-phase flow.

2.1.1 Governing equations

The continuity equation of the mixed fluid flowing in a tubular reactor is

$$\frac{\partial}{\partial t}(\rho_{\mathrm{m}}) + \frac{\partial}{\partial x_i}(\rho_{\mathrm{m}}\boldsymbol{u}_{\mathrm{m}}) = 0. \tag{1}$$

The momentum equation of flow in the inner system of the tubular reactor can be understood as the addition of momentum equation of catalyst particle phase and liquid phase, whose formula is

$$\frac{\partial}{\partial t}\left(\rho_{\mathrm{m}}\vec{u}_{\mathrm{m},i}\right) + \frac{\partial}{\partial x_i}\left(\rho_{\mathrm{m}}\vec{u}_{\mathrm{m},i}\vec{u}_{\mathrm{m},j}\right)$$

$$= -\frac{\partial p}{\partial x_i} + \frac{\partial}{\partial x_j}\mu_{\mathrm{m}}\left(\frac{\partial \vec{u}_{\mathrm{m},i}}{\partial x_j} + \frac{\partial \vec{u}_{\mathrm{m},j}}{\partial x_i}\right)$$

$$+\rho_{\mathrm{m}}g_i + \vec{F}_i + \frac{\partial}{\partial x_i}\left(\alpha_{\mathrm{p}}\rho_{\mathrm{p}}\vec{u}_{\mathrm{dr},i}\vec{u}_{\mathrm{dr},j}\right), \tag{2}$$

$$\vec{u}_{\mathrm{m}} = \frac{\alpha_{\mathrm{p}}\rho_{\mathrm{p}}\vec{u}_{\mathrm{p}} + \alpha_{\mathrm{q}}\rho_{\mathrm{q}}\vec{u}_{\mathrm{q}}}{\rho_{\mathrm{m}}}, \tag{3}$$

$$\rho_{\mathrm{m}} = \alpha_{\mathrm{p}}\rho_{\mathrm{p}} + \alpha_{\mathrm{q}}\rho_{\mathrm{q}}, \tag{4}$$

where u is the mass mean velocity (m/s); $\vec{F}_i$ is volume force (N); ρ_m is mixture density (kg/m^3); u_{dr} is particle phase drift velocity (m/s); and α_p is particle volume fraction.

The drift velocities are expressed by using the algebraic slip formula (ASM) as

$$\vec{u}_{qp} = \frac{(\rho_p - \rho_m) d_p^2}{18\mu_q f_{drag}} \vec{a}, \tag{5}$$

$$\vec{u}_{dr} = \vec{u}_{qp} - \frac{\alpha_q \rho_q \vec{u}_{qp}}{\rho_m}, \tag{6}$$

where $\vec{a}$ is the acceleration of the second phase particle (m/s^2); and f_{drag} is the drag function.

In addition, the flow in the tubular photocatalytic reaction also involves turbulence. Therefore, the turbulence model needs to be added to the mixture model in some flow conditions. The standardized k–ε model is used as the turbulence calculation model in this paper, which is two differential transport equations for k and ε, where k is turbulent kinetic energy and ε is turbulent dissipation rate.

$$\frac{\partial}{\partial t}(\rho k) + \frac{\partial}{\partial x_i}(\rho k u_i) = \frac{\partial}{\partial x_j}\left[\left(\mu + \frac{\mu_t}{\sigma_k}\right)\frac{\partial k}{\partial x_j}\right] + G_k + G_b - \rho\varepsilon - Y_M + S_k, \tag{7}$$

$$\frac{\partial}{\partial t}(\rho \varepsilon) + \frac{\partial}{\partial x_i}(\rho \varepsilon u_i) = \frac{\partial}{\partial x_j}\left[\left(\mu + \frac{\mu_t}{\sigma_\varepsilon}\right)\frac{\partial \varepsilon}{\partial x_j}\right] + C_{1\varepsilon}\frac{\varepsilon}{k}(G_k + C_{3\varepsilon}G_b) - C_{2\varepsilon}\rho\frac{\varepsilon^2}{k} + S_\varepsilon, \tag{8}$$

where G_k is the generation of turbulence kinetic energy due to the mean velocity gradients; G_b is the generation of turbulence kinetic energy due to buoyancy; Y_M is the contribution of the fluctuating dilatation in compressible turbulence to the overall dissipation rate; $C_{1\varepsilon}$, $C_{2\varepsilon}$, and $C_{3\varepsilon}$ are constants. σ_k and σ_ε are the turbulent Prandtl numbers for k and ε; and S_k and S_ε are source terms.

2.1.2 Boundary conditions

For the tubular photocatalytic reactor, uniform velocity is the inlet boundary condition.

$$u_{m,x} = \text{constant}, \tag{9}$$

$$u_{m,y} = u_{m,z} = 0. \tag{10}$$

The turbulence option at the entrance is calculated as

$$k_m = 0.004 u_m^2, \tag{11}$$

$$\varepsilon_m = \frac{0.18 k_m^{1.5}}{0.03D}. \tag{12}$$

For the outlet of the flow model, the pressure condition is used.

$$P_{out} = \text{constant}. \tag{13}$$

For the wall, the slip-free condition is selected in the flow model of the tubular photocatalyst reactor. As to the nearby space, the wall function method is used in the calculation model. As a result of the viscous force, the wall operation needs to be divided into two situations.

1) For the calculated region ($y^* < 11.225$) in the viscous boundary layer, the region is dominated by viscosity. Therefore, the velocity needs to meet

$$u^* = \frac{\rho_m C_{\mu_m}^{0.25} k_p^{0.25} y_p}{\mu_m}. \tag{14}$$

2) For computational areas outside the viscous boundary layer, the velocity is calculated by

$$u^* = 2.3883 \ln(E y^*). \tag{15}$$

2.2 Measurement of catalyst radiation correlation coefficient

The basis and key to establish the radiation model of photocatalytic reaction is to obtain the spectral scattering and absorption coefficient of photocatalyst.

2.2.1 Measurement of extinction coefficient of photocatalyst $Cd_{0.5}Zn_{0.5}S$

First, for the measurement of the extinction coefficient (the sum of absorption and scattering coefficients) of $Cd_{0.5}Zn_{0.5}S$ photocatalyst, Lambert-Beer law can be directly applied [25]. The general mathematical expression for Lambert-Beer law is

$$A = \lg\frac{1}{T} = \beta c L, \tag{16}$$

where A is absorbance, T is transmittance (the ratio of output light intensity I_t to incident light intensity I_0), β is the extinction coefficient, c is the concentration of photocatalyst, t is the extinction time, and L is the thickness of absorption layer. The basic measuring principle of extinction coefficient is demonstrated in Fig. 1.

The simulated light source is the Perfect Light PLS-SXE300 Xenon lamp, with a spectrum range of of 300–2500 nm and an instability of less than ±0.5%. The stirring device is JK-MSH-Ppo-6A magnetic agitator, with a speed precision of 1 rad/min. The ultrasonic instrument is JY92-IIDN ultrasonic signal generator. The instrument for weighing the catalyst is the JA5003B electronic balance.

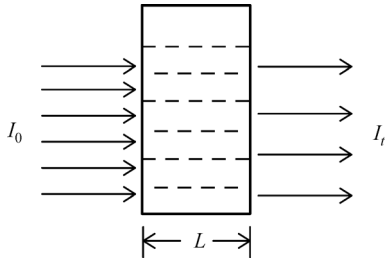

Fig. 1 Schematic diagram of measurement of extinction coefficient for catalyst $Cd_{0.5}Zn_{0.5}S$.

The radiation measuring instrument is LPM-30 power meter.

According to the calculation formula of the Lambert-Beer law, the extinction coefficients of catalyst solutions at different concentrations can be obtained, as listed in Table 1.

Table 1 Extinction coefficient at different catalyst concentrations

Catalyst concentration/$(g \cdot L^{-1})$	Extinction coefficient/$(m^2 \cdot kg^{-1})$
0.25	312.58
0.50	317.31
0.75	327.41

2.2.2 Measurement of absorption coefficient of photocatalyst $Cd_{0.5}Zn_{0.5}S$

The absorption coefficient of photocatalyst $Cd_{0.5}Zn_{0.5}S$ is measured by Cary5000 spectrophotometer of the Agilent Company. The measurement system is illustrated in Fig. 2 [26]. The technical specifications of the spectrophotometer are tabulated in Table 2.

Figure 3 shows the distribution of transmittance with wavelength. Then the average transmittance is calculated through the obtained experimental data, and the absorption coefficients of catalyst solutions at different concentrations are obtained through Eq. (16) as presented in Table 3. After that, the scattering coefficient of catalyst solutions at different concentrations is obtained. The detailed data are given in Table 4.

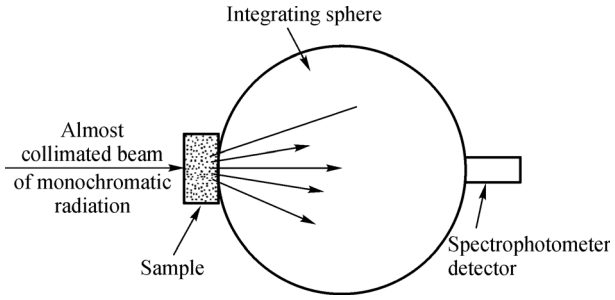

Fig. 2 Schematic diagram of measurement of absorption coefficient for catalyst $Cd_{0.5}Zn_{0.5}S$.

2.3 Radiation model

The shape and specific parameters of the concentrator required in the radiation model can be reffered to in Ref. [27]. The radiation transfer formula (RTE) needs to be solved through a series of processing methods to get the radiation distribution characteristics inside the reactor. RTE is expressed as

$$\frac{\mathrm{d}I_\lambda(s,\Omega)}{\mathrm{d}s} = -\kappa_\lambda I_\lambda(s,\Omega) - \sigma_\lambda I_\lambda(s,\Omega) + \frac{\sigma_\lambda}{4\pi}\int_{\Omega=4\pi} P(\Omega' \rightarrow \Omega) I_\lambda(s,\Omega')\mathrm{d}\Omega', \quad (17)$$

where I_λ is the radiation intensity (W/m^2); s is the coordinate of photocatalyst (m); Ω is the directional solid angle radians; κ_λ is the absorption coefficient; σ_λ is the scattering coefficient; P is the scattering phase function; and λ is the wavelength of light.

The local volume rate of photon absorption (LVRPA) is often used to evaluate the radiation field and the spatial distribution of radiation absorption in photocatalytic reactors. LVRPA is used as the index of radiation absorption level and optimization of the photocatalytic system, which can be calculated as

Table 2 Technical specifications for spectrophotometer

Measurement model	Wavelength scanning, time scanning, absorbance measurement
Wavelength range	175–3300 nm (the host), 200–2400 nm (integrating sphere)
Wavelength accuracy	$\leqslant \pm 0.08$ nm (UV/visible region), $\leqslant \pm 0.4$ nm (near infrared)
Wavelength repeatability	$\leqslant \pm 0.005$ nm (UV/visible region), $\leqslant \pm 0.02$ nm (near infrared)
Photometric accuracy	± 0.00025 A
Photometer repeatability	$\leqslant 0.00014$ A
Baseline stability	$\leqslant 0.0001$ Abs/h
The light source	Deuterium lamp, life 2000 h Tungsten lamp, life 3000 h, automatic switch

$$\mathrm{LVRPA}_{(r,\theta)}=\frac{I_{\mathrm{in}}[(\omega_{\mathrm{c}}-1+\sqrt{1-\omega_{\mathrm{c}}^2})\mathrm{e}^{-Dr/\lambda_{\omega}}+\Gamma(\omega_{\mathrm{c}}-1-\sqrt{1-\omega_{\mathrm{c}}^2})\mathrm{e}^{Dr/\lambda_{\omega}}]}{\lambda_{\omega}\omega_{\mathrm{c}}(1-\Gamma)}, \tag{18}$$

where the optical thickness, the extinction length, and the scattering reflectivity are expressed as

$$\Gamma=\frac{1-\sqrt{1-\omega_{\mathrm{c}}^2}}{1+\sqrt{1-\omega_{\mathrm{c}}^2}}\mathrm{e}^{-2\tau_{\mathrm{app}}}, \tag{19}$$

$$\lambda_{\omega}=\left[a(\sigma+\kappa)C_{\mathrm{cat}}\sqrt{1-\omega_{\mathrm{c}}^2}\right]^{-1}, \tag{20}$$

$$\omega_{\mathrm{c}}=\frac{(\omega P_{\mathrm{b}}+4\omega^2P_{\mathrm{s}}^2)/(1-\omega P_{\mathrm{f}}-\omega P_{\mathrm{b}}-2\omega P_{\mathrm{s}})}{(1-\omega P_{\mathrm{f}}-4\omega^2P_{\mathrm{s}}^2)/(1-\omega P_{\mathrm{f}}-\omega P_{\mathrm{b}}-2\omega P_{\mathrm{s}})}, \tag{21}$$

$$\omega=\frac{\sigma}{\sigma+\kappa}, \tag{22}$$

$$\tau_{\mathrm{app}}=\frac{1-\omega P_{\mathrm{f}}-4\omega^2P_{\mathrm{s}}^2}{1-\omega P_{\mathrm{f}}-\omega P_{\mathrm{b}}-2\omega P_{\mathrm{s}}}(\sigma+\kappa)C_{\mathrm{cat}}\Delta\sqrt{1-\omega_{\mathrm{c}}^2}, \tag{23}$$

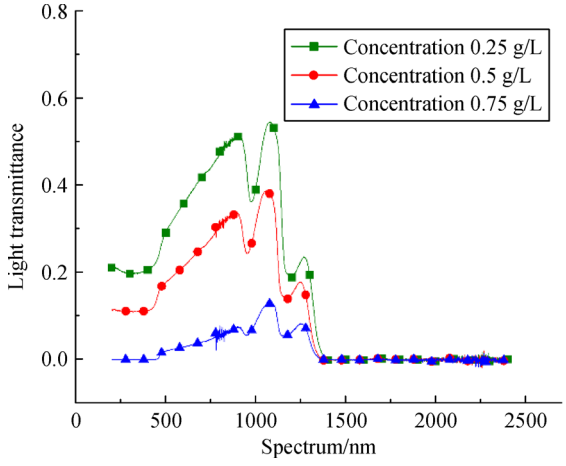

Fig. 3 Distribution of transmittance with wavelength.

Table 3 Absorption coefficients at different catalyst concentrations

Catalyst concentration/(g·L^{-1})	Absorption coefficients/(m^2·kg^{-1})
0.25	304.84
0.5	192.31
0.75	222.36

Table 4 Scattering coefficients at different catalyst concentrations

Catalyst concentration/(g·L^{-1})	Scattering coefficients/(m^2·kg^{-1})
0.25	7.75
0.5	125.00
0.75	105.05

where κ and σ are the absorption and scattering coefficients of catalyst suspensions respectively (m^2/kg); C_{cat} is the local catalyst concentration (g/L); P_{b}, P_{f}, and P_{s} are the probability of scattering backward, forward and sideways respectively; r is the radius of the straight pipe; and Δ is the total distance for the light propagation in tube (m).

Figure 4 exhibits the parameters of LVRPA calculated in a circular tube for the six-flux model.

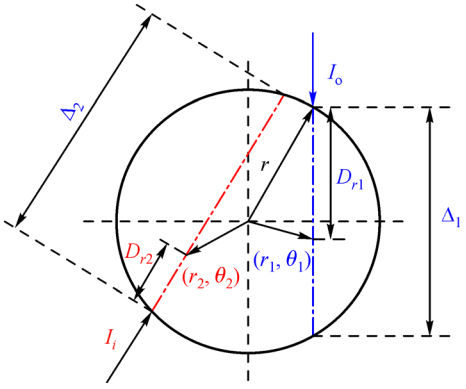

Fig. 4 Schematic diagram of calculation parameters in six-flux model.

3 Model validation

3.1 Flow model validation

3.1.1 Meshing

The geometric model in this paper is a circular straight pipe with a radius of 20 mm and a length of 2500 mm. The mesh is drawn by ICEM and the structured meshing is adopted, as depicted in Fig. 5. The mesh independence in the tubular reactor is verified through five different grid densities (up to six times). It can be seen in Fig. 6 that the core parameter-catalyst concentration distribution will not change with the change of mesh density. The mesh with a density of 2.4×10^5 is selected after mesh independence verification.

3.1.2 Parameter settings

In this paper, ANSYS16.0 is used for calculation. In the process of solution, the case is calculated by SIMPLEC algorithm and the second-order windward integral. The iteration error is set to 10^{-6}. The main physical parameters involved in the simulation calculation are summarized in Table 5.

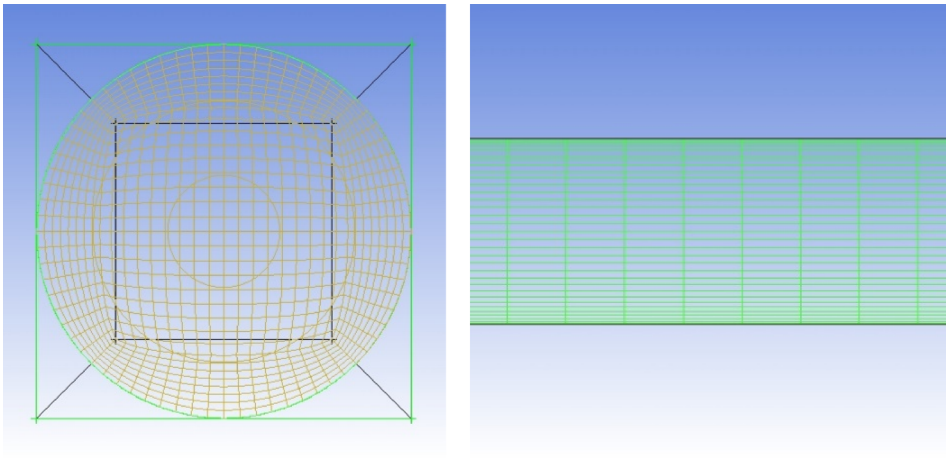

(a) (b)

Fig. 5 Meshing diagram for circular straight pipe.
(a) Meshing diagram for circular straight pipe cross section; (b) meshing diagram for circular straight pipe longitudinal section.

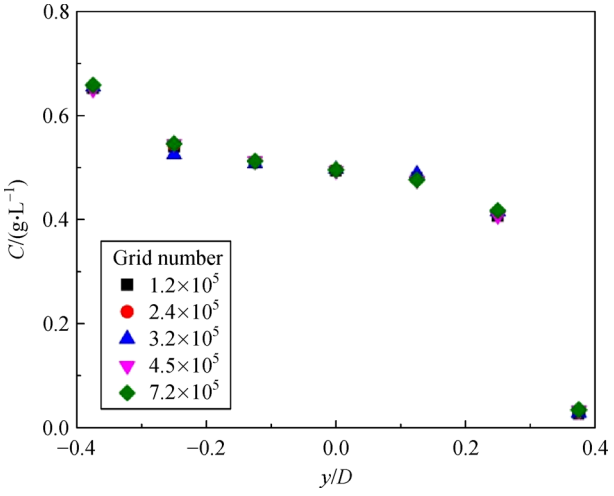

Fig. 6 Mesh independence verification in tubular reactor.

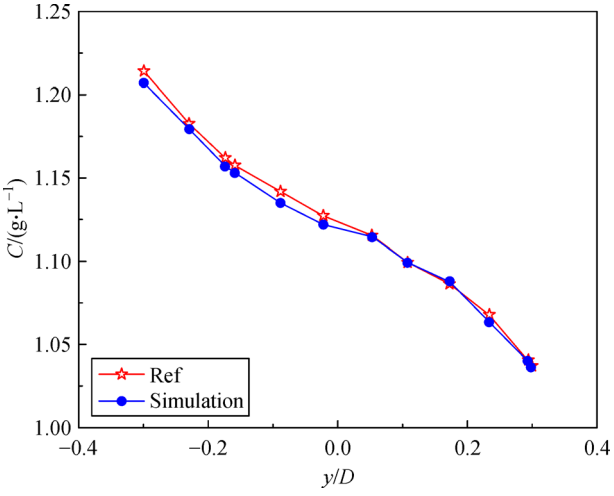

Fig. 7 Verification of the mixture model in tubular reactor.

3.1.3 Model validation

To verify the accuracy of the flow model in this paper, a group of working conditions in Ref. [13] is simulated and solved. The parameter settings are shown in Table 6, and the compared simulation results are manifested in Fig. 7. A comparison of the data suggests that the maximum relative error is 0.61%, which proves that the mixture model adopted in this paper is reasonable and effective under the conditions described in Ref. [13].

Table 5 Related parameters in simulation calculation

Parameter	Setting value
Tube radius/m	0.02
Tube length/m	2.5
Tube inclination/(°)	45
Fluid density/(kg·m^{-3})	998.2
Catalyst particle density/(kg·m^{-3})	4800
Catalyst particle radius/μm	10

3.2 Radiation model validation

Colina-Márquez et al. [28] used the radiation model to simulate the internal radiation distribution of the tubular reactor containing TiO_2 particle suspension. To verify the correctness of the radiation model in this paper, the radiation conditions in Ref. [28] are simulated and solved. The parameter settings are shown in Table 7, and the compared simulation results are displayed in Fig. 8.

The radiation model in this paper is adopted to calculate LVRPA, and the radiation distribution in the tube is plotted in Fig. 8(b). It can be seen from Figs. 8(a) and 8(b) that the

Table 6 Parameter settings in Ref. [13]

Parameter	Setting value
Tube radius/m	0.03
Tube length/m	1.5
Tube inclination	Horizontal
Fluid density/(kg·m^{-3})	1000
Catalyst particle density/(kg·m^{-3})	4800
Catalyst particle radius/μm	10

Table 7 Parameter settings in Ref. [28]

Parameter	Value
Catalyst concentration/(g·L^{-1})	0.5
Received tube diameter/mm	33.0
Reflectivity of condenser	0.85
Concentrator receiving half angle/(°)	90.0
Top-bottom clearance of concentrator/mm	0.0
Incident radiation intensity/(W·m^{-2})	30.0
Catalyst solution absorption coefficient/(m^2·kg^{-1})	174.75
Catalyst solution scattering coefficient/(m^2·kg^{-1})	1295.75
Forward scattering probability	0.11
Backward scattering probability	0.74
Side scattering probability	0.045

radiation distribution of the top and middle half of the tube calculated by the optimized six-flux radiation model in this paper is similar to that in Ref. [28], except the radiation distribution at the bottom of the tube. However, according to the actual situation, when the incident light is far away from the receiver tube, there should be radiation intensity at the bottom of the actual receiver tube. However, since there is no radiation at the bottom of the receiver tube in Fig. 8(a), the radiation model in this paper is closer to the reality.

4 Results and discussion

4.1 Flow model

When the photocatalyst is transported in the circular tube reactor under the combined action of gravity, shear force, and other forces, the catalyst particles would form a certain distribution trend. Gravity would make the catalyst particles settle down, while under the action of flow, the particles would keep suspended. Therefore, when the inlet velocity is too small, the effect of turbulent force on catalyst particles in the reactor is not obvious, which would make particles sink and even form deposition. In addition, at the same inlet flow velocity, different catalyst distributions could be obtained due to the different initial concentrations of the catalyst. When the fluid flows into the reactor, at the inlet stage, the fluid properties in this stage are different from those in the subsequent stage, such as the thin boundary layer. Because the flow is not fully developed, this phenomenon is called the inlet effect in science. To eliminate the effect of inlet effect, the distribution of catalyst concentration in the outlet cross-section of the fluid is studied in this paper.

4.1.1 Flow distribution at different catalyst concentrations

Under the condition of the same inlet flow velocity, the change of photocatalytic concentration would show different types of distributions. The parameters of the simulated flow conditions are shown in Table 8.

In the tubular reactor, the distributions of catalyst at the outlet of the reactor are shown in Fig. 9 at different catalyst concentrations at the inlet of the reactor.

In the case of the same inlet velocity and three different catalyst concentrations in the round tubular photocatalytic reactor, the comparison and analysis of the catalyst particle concentration along the radial direction at the outlet cross-section is shown in the Fig. 10. As can be seen

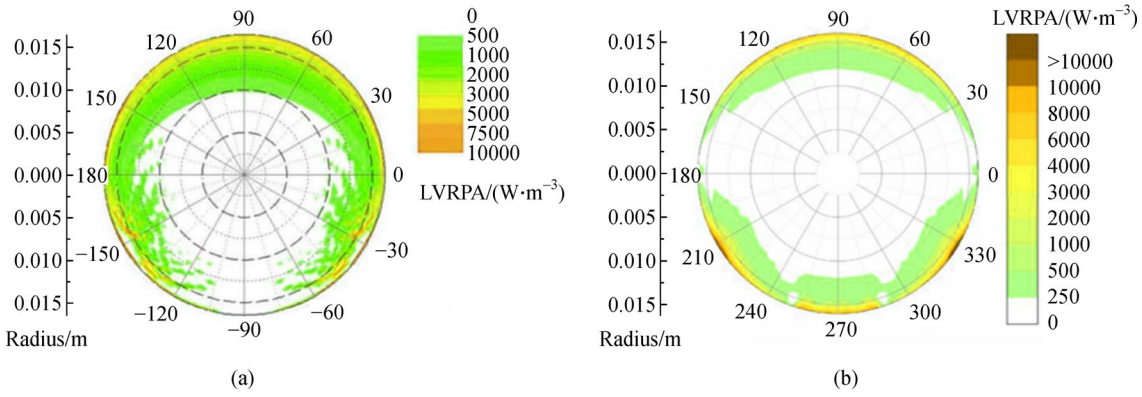

Fig. 8 Comparison of radiation model.
(a) Radiation distribution in the reference; (b) radiation distribution of radiation model used in this paper.

Table 8 Parameters at different catalyst concentrations

Flow velocity/(m·s^{-1})	Concentration 1/(g·L^{-1})	Concentration 2/(g·L^{-1})	Concentration 3/(g·L^{-1})
0.28	0.25	0.5	0.75

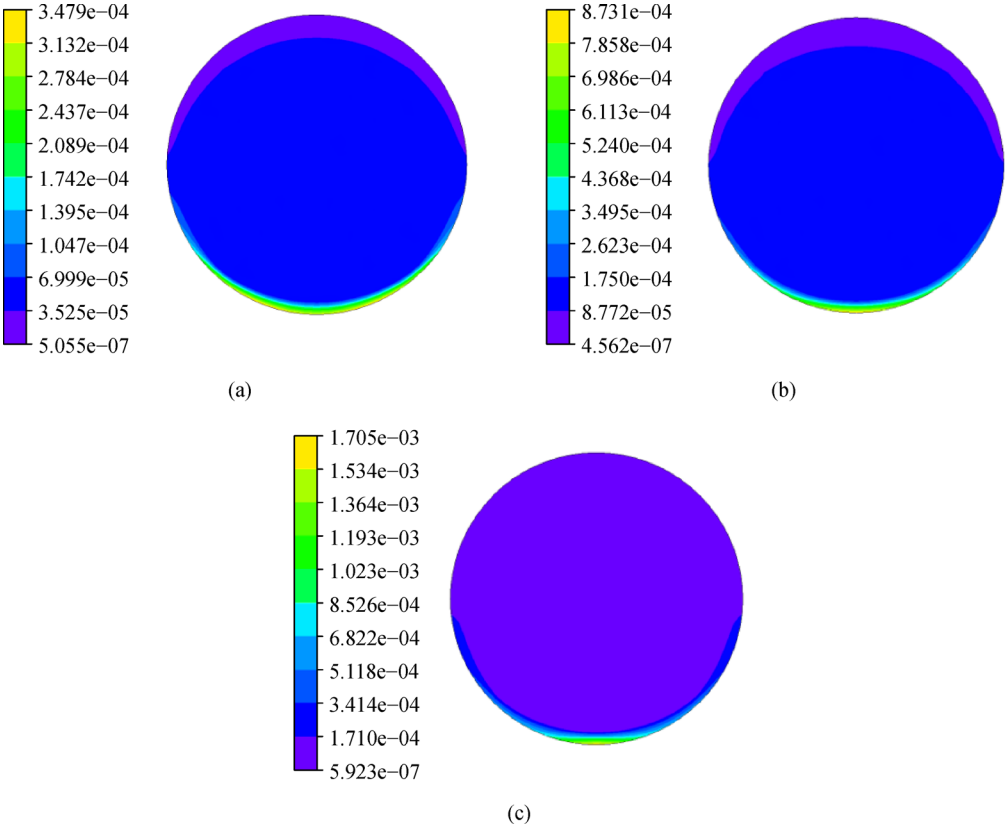

Fig. 9 Cloud diagrams of catalyst concentration distributions at the outlet of reactor. (a) Concentration 1; (b) concentration 2; (c) concentration 3.

from Fig. 10, when the inlet flow velocity is 0.28 m/s, for the selected catalyst concentrations, a certain catalyst deposition and accumulation would be formed at the exit section of the tubular photocatalytic reactor. For the three flow conditions, the photocatalyst concentration at the top of the pipeline is almost zero, while the catalyst sedimentation effect reaches its peak at the bottom of the tubular reactor, and the maximum catalyst concentration also appears. With the increase of the concentration of the catalyst at the inlet, the concentration of the catalyst increases: when the initial concentration is 0.25 g/L, the photocatalyst concentration at the bottom of the pipeline is 1.55 g/L; when the initial concentration is 0.5 g/L, the photocatalyst concentration at the bottom of the pipeline is 4.19 g/L; and when the initial concentration is 0.75 g/L, the photocatalyst concentration at the bottom of pipeline is 8.18 g/L. In addition, as the inlet catalyst concentration increases, the catalyst concentration increases at the same position in the tubular reactor, but the overall distribution in the central region is relatively uniform and the difference is not great, but the distributions show greater differences at the bottom and the top of the pipe, mainly due to the influence of gravity.

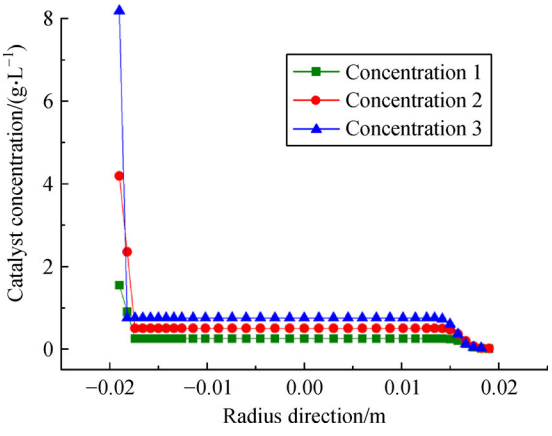

Fig. 10 Comparison of catalyst concentration distributions at the outlet of reactor at different catalyst concentrations.

Based on the above analysis, it is found that the central distribution of the tubular photocatalytic reactor is uniform, and the distributions of the two ends are uneven. With the increase of the inlet photocatalytic concentration, the photocatalyst concentration of the outlet cross-section increases accordingly.

4.1.2 Flow distribution at different flow velocities

At the same catalyst concentration, the different inlet flow velocities show different distribution patterns. The parameters of simulated flow conditions are provided in Table 9. Inside the tubular reactor, at different inlet flow velocities, the distributions of the catalyst at the reactor outlet are shown in Fig. 11. In the case of the same catalyst concentration and three different inlet flow velocities at the inlet of the tubular photocatalytic reactor, the comparative analysis figures of catalyst particle concentration at the outlet section along the radius are shown in Fig. 11. As can be seen from Fig. 11 that when the concentration of catalyst at the inlet is 0.5 g/L, for the selected flow velocities, certain catalyst deposition and accumulation would still be formed at the exit section of the tubular photocatalytic reactor. For the three flow conditions, the photocatalyst concentration at the top of the pipe is almost zero, while the catalyst deposition effect reaches the peak at the bottom of the round tubular reactor, and the maximum catalyst concentration also appears and decreases with the increase of the inlet velocity: when the initial velocity is 0 m/s, the photocatalyst concentration at the bottom of pipeline is 25.06 g/L; when the initial velocity is 0.14 m/s, the photocatalyst concentration at the bottom of the pipeline is 9.88 g/L; and when the initial velocity is 0.28 m/s, the photocatalyst concentration at the bottom of the pipeline is 4.19 g/L. In addition, it can be seen that the initial velocity in the pipe is 0 m/s, i.e., the inner flow of the tubular reactor is a natural circulation mode, the catalyst distribution at the outlet section of the pipe is extremely uneven. Because there is no turbulence

Table 9 Parameters at different flow velocities

Concentration/(g·L^{-1})	Flow velocity 1/(m·s^{-1})	Flow velocity 2/(m·s^{-1})	Flow velocity 3/(m·s^{-1})
0.5	0	0.14	0.28

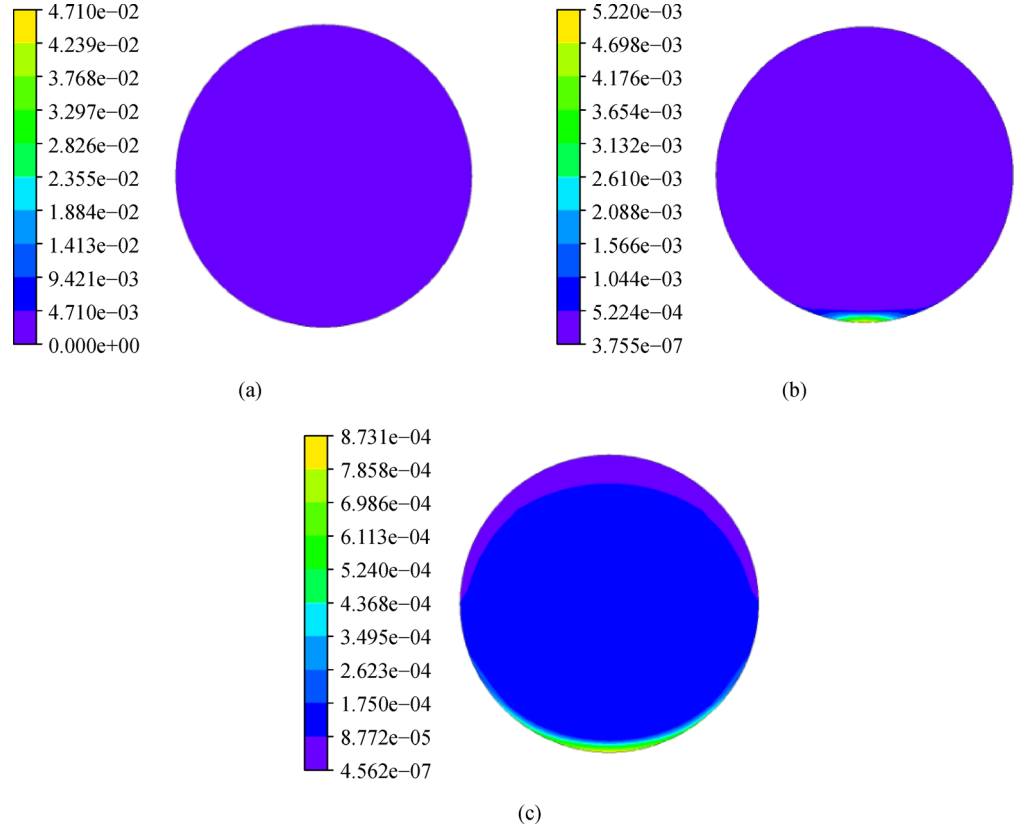

Fig. 11 Cloud diagrams of catalyst concentration distributions at the outlet of reactor.
(a) Flow velocity 1; (b) flow velocity 2; (c) flow velocity 3.

disturbance, most of the catalyst particles are accumulated at the outlet to the bottom of the pipe, and the others are rarely distributed. As the inlet velocity increases gradually, the catalyst concentration becomes uniform at the same position in the tubular reactor, and the turbulent force increases with the increase of the flow velocity, which makes the distribution of catalyst in the pipe become uniform.

Based on the above analysis, it appears that the distribution of catalyst in the outlet section of the tubular photocatalytic reactor is greatly influenced by the inlet velocity, and with the increase of the inlet velocity, the distribution of the catalyst at the outlet is relatively uniform. The maximum concentration of the pipeline relatively decreases, which reduces the deposition effect.

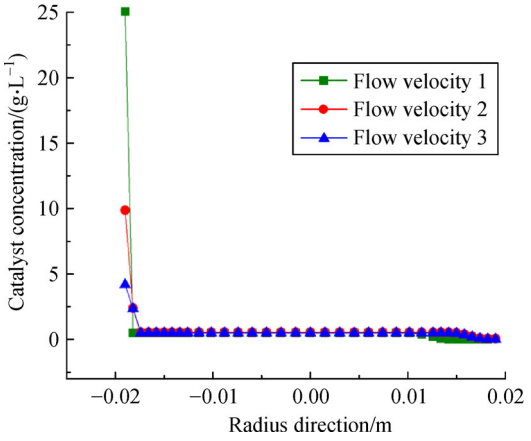

Fig. 12 Comparison of catalyst concentration distributions at the outlet of reactor at different inlet velocities.

4.2 Radiation model

4.2.1 Radiation distribution at different catalyst concentrations

At the same inlet flow velocity, the change of the photocatalytic concentration has a different radiation distribution. The parameters of specific simulated flow conditions are shown in Table 8. Inside the tubular reactor, at different catalyst concentrations in the inlet, the cloud diagrams of the radiation distribution at the outlet of the reactor are shown in Fig. 13. At the same inlet flow velocity and three different photocatalyst concentrations, it can be seen from the cloud images that when the cycle speed is 0.28 m/s, at concentration 1, the radiation distribution at the outlet of the tubular photocatalytic reactor is more uniform than that at concentrations 2 and 3 due to the low concentration of the catalyst, and the fact that the flow velocity could make the catalyst achieve a certain degree of suspension. Then, with the increasing concentration of catalyst at concentrations 2 and 3, the deposition effect of the catalyst gradually increases with a constant cycle speed, which makes the radiation distribution non-uniform. In addition, most of the radiation energy gradually begins to accumulate toward the bottom of the reactor tube. With the increase of catalyst concentration, the radiation energy becomes uneven, but the whole radiation distribution energy is increasing. From the cloud images, it can be seen that the maximum energy is 2.0×10^5 W/m^3 at concentration 1. On the other hand, compared to concentration 1, the maximum energy of concentrations 2 and 3 increases by 1150% and 1900%, respectively, reaches 2.5×10^6 W/m^3 and 4.0×10^6 W/m^3, respectively.

The above analysis indicates that the radiation distribution in the outlet cross section of the tubular photocatalytic reactor is greatly influenced by the catalyst concentration. With the increase of the catalyst concentration, the radiation distribution in the pipeline becomes uneven at the outlet of the reactor, and begins to accumulate toward the bottom of the reactor, but the radiation value gradually increases.

4.2.2 Radiation distribution at different flow velocities

At the same catalyst concentration, the inlet flow velocity change would show different radiation distribution rules. The parameters of specific simulated flow conditions are shown in Table 9. Inside the tubular reactor, at different flow velocities at the inlet, the radiation distribution cloud diagrams at the reactor outlet are shown in Fig. 14. In the case of the same concentration inlet catalyst and three different inlet flow velocities in the round tubular photocatalytic reactor, it could be seen from the cloud charts that when the concentration of the photocatalyst is 0.5 g/L, for the three flow velocities, since the photocatalyst is not to be fully suspended, most of the energy is concentrated at the bottom of the reactor tube. Compared with flow velocities 1 and 2, the radiation distribution of flow velocity 3 at the outlet of the circular tubular photocatalytic reactor tends to disperse in all directions, and there is no excessive concentration of energy density as far as flow velocities 1 and 2 are concerned due to the fact that the flow velocity is not enough to make the catalyst suspend, but with the increase of the flow velocity, the catalyst tends to suspend. Then, with the decrease of the flow velocity at concentrations 1 and 2, the deposition effect of the catalyst gradually increases, which makes the radiation distribution become more concentrated. With the decrease of the flow velocity, the radiation energy becomes more concentrated toward the bottom of the tube, but the overall radiation distribution energy is increasing. It could be seen from the cloud charts that the maximum energy is 2.5×10^6 W/m^3 at flow velocity 3, while compared with flow velocity 3, the flow velocities 1 and 2 increase by 284% and 220%, respectively, reaching 9.6×10^6 W/m^3

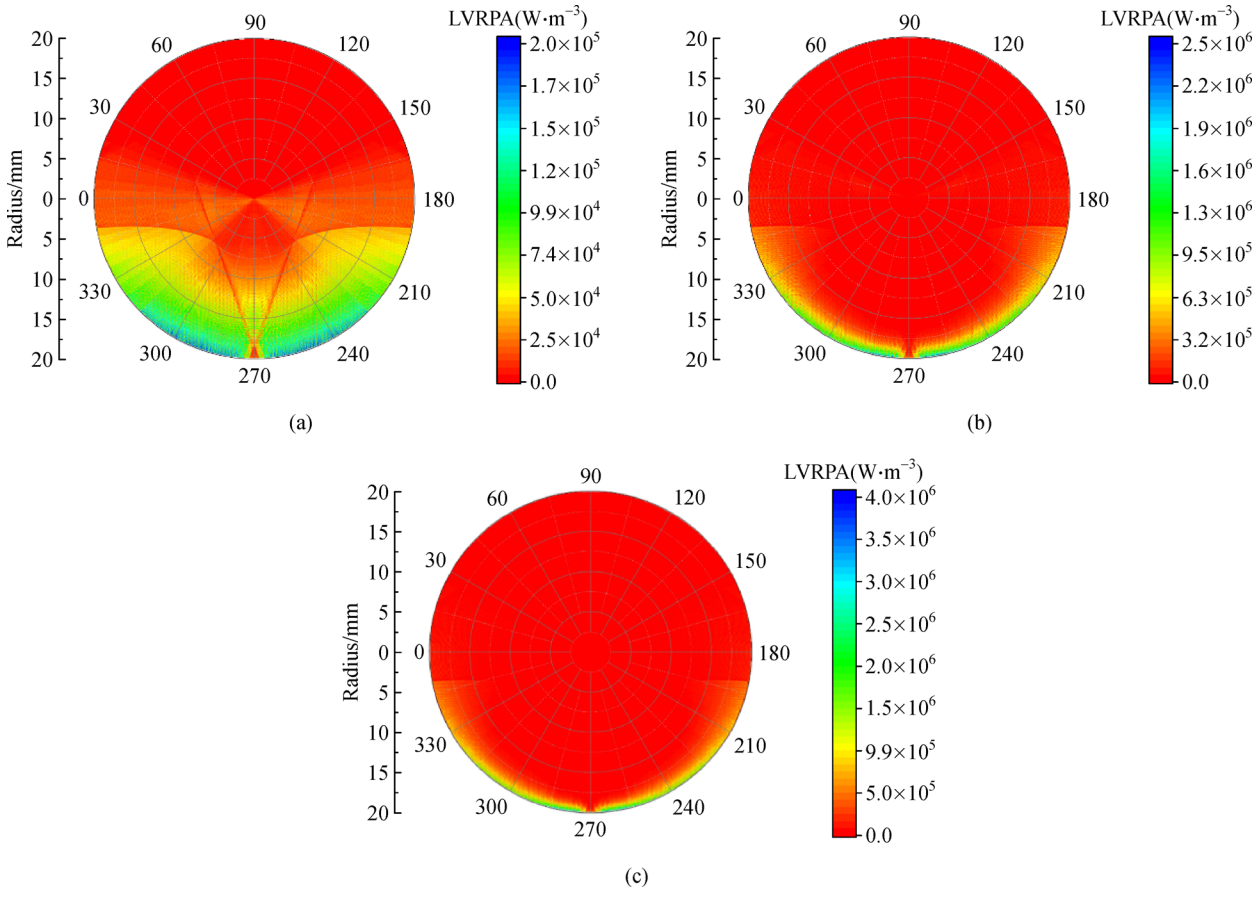

Fig. 13 Cloud diagrams of radiation distribution at the outlet of reactor.
(a) Concentration 1; (b) concentration 2; (c) concentration 3.

and 8 × 10^6 W/m^3.

The above analysis suggests that the radiation distribution in the outlet cross section of the tubular photocatalytic reactor is greatly affected by the inlet flow velocity. With the decrease of the flow velocity, the radiation distribution at the outlet of the reactor is more concentrated at the bottom of the reactor pipe, but the radiation value is gradually increasing.

5 Conclusions

5.1 Flow model

The distribution law and data of the photocatalyst in the outlet section under different flow conditions are obtained, and the following main conclusions are reached:

Circular tubular photocatalytic reactor has a uniform distribution in the central region and uneven distributions at both ends, and the photocatalyst concentration at the outlet section increases correspondingly with the increase in the inlet photocatalytic concentration.

With the increase of the inlet velocity, the distribution of the catalyst at the outlet is more uniform, and the maximum concentration of the pipeline is relatively reduced, which reduces the effect of deposition.

5.2 Radiation model

A radiation model is established in the round tubular photocatalytic reactor. Combining with the radiation model, the radiation distribution characteristics under different flow fields are compared and analyzed. The main conclusions are as follows:

The spectral extinction (sum of scattering and absorption) and absorption coefficient of $Cd_{0.5}Zn_{0.5}S$ photocatalyst are obtained.

As the concentration of catalyst increases, the radiation distribution in the pipeline becomes uneven at the reactor outlet and begins to accumulate toward the bottom of the reactor, but the radiation value gradually increases.

With the decrease of flow velocity, the radiation distribution in the pipeline is more concentrated toward the bottom of the reactor, but the radiation value is gradually increasing.

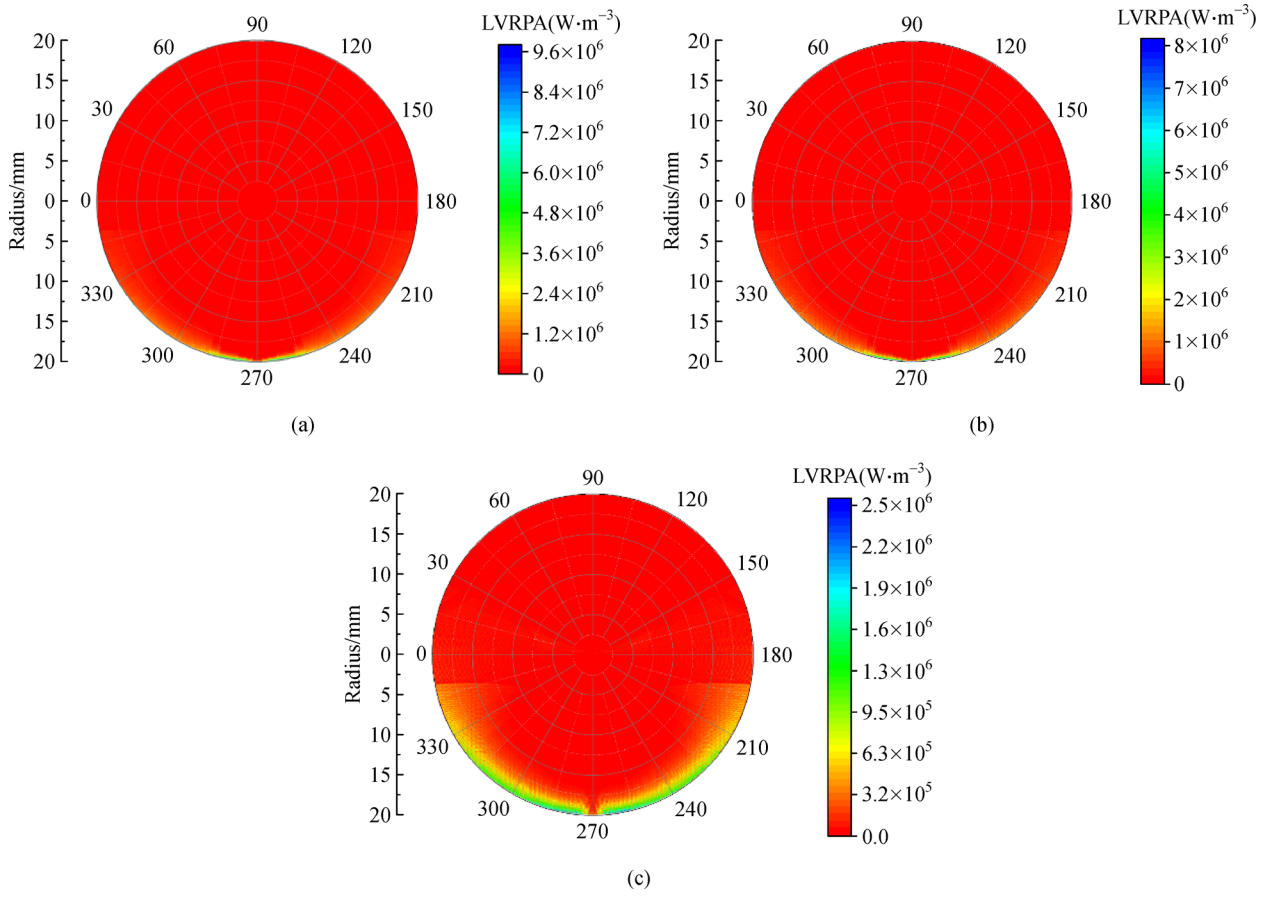

Fig. 14 Cloud diagrams of radiation distribution at the outlet of the reactor. (a) Flow velocity 1; (b) flow velocity 2; (c) flow velocity 3.

Acknowledgements This work was supported by the National Key Research and Development Program of China (No. 2018YFB1502005), the National Natural Science Foundation of China (Grant Nos. 51961130386 and 51506043), the Royal Society-Newton Advanced Fellowship grant (NAF/R1/191163), the National High Technology Research and Development Program of China (No. 2012AA051501), and the Foundation of the State Key Laboratory of Multiphase Flow in Power Engineering, Xi'an Jiaotong University, China.

References

1. Chen X, Shen S, Guo L, et al. Semiconductor-based photocatalytic hydrogen generation. Chemical Reviews, 2010, 110(11): 6503–6570
2. Grätzel M. Photoelectrochemical cells. Nature, 2001, 414(6861): 338–344
3. Lewis N S. Light work with water. Nature, 2001, 414(6864): 589–590
4. Lewis N S. Toward cost-effective solar energy use. Science, 2007, 315(5813): 798–801
5. Lewis N S, Crabtree G. Basic research needs for solar energy utilization. Report of the Basic Energy Sciences Workshop on Solar Energy Utilization. Washington DC, Office of Basic Energy Science, US Department of Energy, 2005
6. Walter M G, Warren E L, McKone J R, et al. Solar water splitting cells. Chemical Reviews, 2010, 110(11): 6446–6473
7. Züttel A, Borgschulte A, Schlapbach L. Hydrogen as a Future Energy Carrier. Wiley-VCH Verlag GmbH & Co. KGaA, 2008
8. Chornet E, Czernik S. Harnessing hydrogen. Nature, 2002, 418(6901): 928–929
9. Schlapbach L. Hydrogen-fueled vehicles. Nature, 2009, 460(7257): 809–811
10. Xia Z. Solar-powered hydrogen production clean energy supply system. Solar Energy, 1994, (3): 31 (in Chinese)
11. Kumar J, Bansal A. Photocatalytic degradation in annular reactor: modelization and optimization using computational fluid dynamics (CFD) and response surface methodology (RSM). Journal of Environmental Chemical Engineering, 2013, 1(3): 398–405
12. Ren Y, Jing D. Study on particle and photonic flux distributions in a magnetically stirred photocatalytic reactor. Journal of Photonics for Energy, 2015, 5(1): 052097
13. Ren Y, Zhao L, Jing D, et al. Investigation and modeling of CPC based tubular photocatalytic reactor for scaled-up hydrogen production. International Journal of Hydrogen Energy, 2016, 41(36): 16019–16031
14. Casado C, Marugán J, Timmers R, et al. Comprehensive multi-

physics modeling of photocatalytic processes by computational fluid dynamics based on intrinsic kinetic parameters determined in a differential photoreactor. Chemical Engineering Journal, 2017, 310: 368–380

15. Acosta-Herazo R, Monterroza-Romero J, Mueses M Á, et al. Coupling the six flux absorption-scattering model to the henyey-greenstein scattering phase function: evaluation and optimization of radiation absorption in solar heterogeneous photoreactors. Chemical Engineering Journal, 2016, 302: 86–96
16. Moreno-SanSegundo J, Casado C, Marugán J. Enhanced numerical simulation of photocatalytic reactors with an improved solver for the radiative transfer equation. Chemical Engineering Journal, 2020, 388: 124183
17. Peralta Muniz Moreira R, Li Puma G. Multiphysics computational fluid-dynamics (CFD) modeling of annular photocatalytic reactors by the discrete ordinates method (DOM) and the six-flux model (SFM) and evaluation of the contaminant intrinsic kinetics constants. Catalysis Today, 2021, 361: 77–84
18. Ramírez-Cabrera M A, Valadés-Pelayo P J, Arancibia-Bulnes C A, et al. Validity of the six-flux model for photoreactors. Chemical Engineering Journal, 2017, 330: 272–280
19. Cassano A E, Alfano O M. Reaction engineering of suspended solid heterogeneous photocatalytic reactors. Catalysis Today, 2000, 58(2–3): 167–197
20. Roupp G B, Nico J A, Annangi S, et al. Two-flux radiation-field model for an annular packed-bed photocatalytic oxidation reactor. AIChE Journal, 1997, 43(3): 792–801
21. Cao F, Li H, Chao H, et al. Optimization of the concentration field in a suspended photocatalytic reactor. Energy, 2014, 74(5): 140–146
22. Romero R L, Alfano O M, Cassano A E. Cylindrical photocatalytic reactors. Radiation absorption and scattering effects produced by suspended fine particles in an annular space. Industrial & Engineering Chemistry Research, 1997, 36(8): 3094–3109
23. Jing D, Jing L, Liu H, et al. Photocatalytic hydrogen production from refinery gas over a fluidized-bed reactor II: parametric study. Industrial & Engineering Chemistry Research, 2013, 52(5): 1992–1999
24. Brucato A, Cassano A E, Grisafi F, et al. Estimating radiant fields in flat heterogeneous photoreactors by the six-flux model. AIChE Journal, 2006, 52(11): 3882–3890
25. Marinangeli R E, Ollis D F. Photoassisted heterogeneous catalysis with optical fibers: I. Isolated single fiber. AIChE Journal, 1977, 23 (4): 415–426
26. Cabrera M I, Alfano O M, Cassano A E. Absorption and scattering coefficients of titanium dioxide particulate suspensions in water. Journal of Physical Chemistry, 1996, 100(51): 20043–20050
27. Wei Q, Yang Y, Liu H, et al. Experimental study on direct solar photocatalytic water splitting for hydrogen production using surface uniform concentrators. International Journal of Hydrogen Energy, 2018, 43(30): 13745–13753
28. Colina-Márquez J, Machuca-Martínez F, Puma G L. Radiation absorption and optimization of solar photocatalytic reactors for environmental applications. Environmental Science & Technology, 2010, 44(13): 5112–5120